

C2PO: Coherent Co-packaged Optics using offset-QAM-16 for Beyond PAM-4 Optical I/O

DAN STURM^{1,*}, MARZIYEH REZAEI¹, ALANA DEE¹, AND SAJJAD MOAZENI¹

¹Department of Electrical and Computer Engineering, University of Washington, Seattle, WA, 98195, USA

*dansturm@uw.edu

Compiled June 17, 2025

Co-packaged optics (CPO) has emerged as an ultimate solution for achieving the ultra-high bandwidths, shoreline densities, and energy efficiencies required by future GPUs and network switches for AI. Microring modulators (MRMs) are well-suited for transmitters due to their compact size, high energy efficiency, and natural compatibility for dense wavelength-division multiplexing (DWDM). However, extending beyond the recently-demonstrated 200 Gb/s will require more advanced modulation formats such as higher-order coherent (e.g., QAM-16).

In this work, we show how microring resonators (MRMs) can be efficiently used to implement phase-constant amplitude modulators and form the building blocks of a transmitter for offset-QAM-16, which has been shown to simplify carrier-phase recovery relative to QAM with no offset. We simulate and evaluate the performance of our proposed MRM-based coherent CPO (C2PO) transmitters using a foundry-provided commercial silicon photonics process, demonstrating an input-normalized electric field amplitude contrast of 0.64 per dimension. Through full link-level bit error rate modeling, we show that our design achieves 400 Gb/s using offset-QAM-16 at a total optical laser power of 9.65 dBm—comparable to that required by conventional QAM-16 MZI-based links—despite using 10–100× less area. We further conduct a thermal simulation to assess the transmitter’s thermal stability at the MRM input optical power required to meet a target BER at the desired data rates. Finally, as a proof of concept, we demonstrate 25 Gb/s MRM-based offset-QAM-4 modulation with a chip fabricated in the GlobalFoundries 45 nm monolithic silicon photonics process.

<http://dx.doi.org/10.1364/ao.XX.XXXXXX>

1. INTRODUCTION AND RELATED WORK

As AI/ML accelerators, GPUs, and network switches increasingly demand tens of Tb/s of off-package IO bandwidth at pJ/bit efficiencies and 1+ Tb/s/mm shoreline densities, the adoption of co-packaged optics (CPO) is becoming inevitable [1]. Although today’s pluggable optical modules use Mach-Zehnder Modulator (MZM)-based transmitters [2], their large footprint (multi-mm) bottlenecks shoreline density for CPO and prevents them from reaching the limits imposed by fiber pitch. Hence, CPO will rely on microring modulators (MRMs) as electro-optical transmitters. While the compact footprint of these devices (10s of μm s) enables high density, overall shoreline density will still be limited by the pitch of fibers used to take optical signals off package (Fig 1a, b). Thus, the future of CPO and shoreline density scaling will rely on increasing the datarate per fiber of MRM-based transmitters.

MRM-based transmitters currently utilize only amplitude modulation, such as pulse amplitude modulation (PAM) (e.g.,

NRZ and PAM-4). Wavelength division multiplexing (WDM) has been proposed to achieve higher shoreline densities and is naturally suitable for MRMs due to their wavelength selectivity [4]. However, with conventional MRM datarates of 32 or even 100 Gb/s/lane, system performance will be limited by the large number of WDM lines required for meeting target densities, given the challenges of making high-quality multi-wavelength laser sources and managing the thermal sensitivity of MRMs (Fig. 1b). Meanwhile, scaling with polarization division multiplexing (PDM) is also plausible, however this is limited by physics and also requires more expensive polarization maintaining (PM) fibers and assembly. Therefore, reaching 200 or 400 Gb/s per wavelength is becoming a must to meet the future shoreline densities provided by advanced die-to-die interconnects like 3D UCIE [5]. However, scaling the baud rate beyond 100 Gbd is extremely challenging as CMOS scaling no longer improves the mixed-signal circuit performance. Achieving energy-efficient higher data rates per lane to increase shoreline density will thus require more advanced coherent modulations.

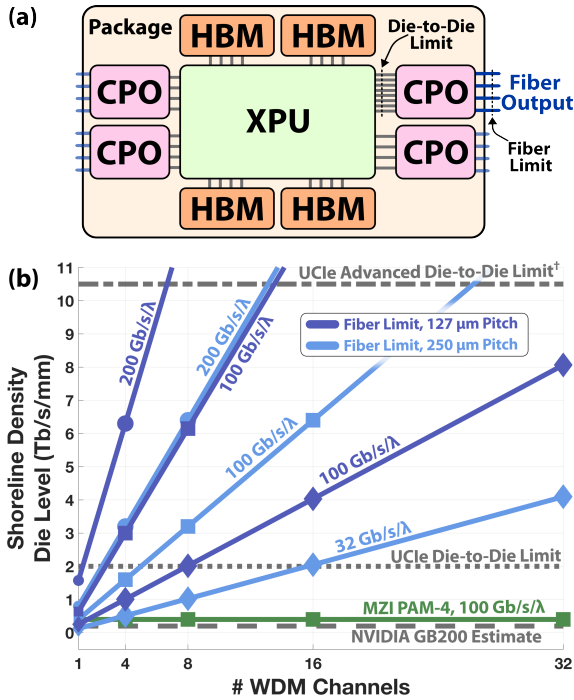


Fig. 1. (a) Illustration of future System-in-Package (SiP) with CPO for optical I/O, and (b) die-level shoreline density comparison and requirements for CPO solutions at standard fiber pitches of 127 or 250 μm .

†The UCIe 1.0 Advanced spec is for 2.5D packaging, i.e. dies connected with a silicon bridge or interposer [3]

Building MRM-based QAM-16 transmitters can increase the data rate to 200 or 400 Gb/s without using more laser lines or increasing the baud rate, and can thus be an ultimate solution for future CPO. Although coherent optics using quadrature amplitude modulation (QAM) has been widely used for long-haul (+10km) applications with Mach-Zehnder modulator (MZM)-based transmitters [6], it is extremely challenging with MRMs due to the coupled nature of their phase and amplitude outputs.

Coherent MRM-based transmitters have previously been demonstrated in the form of single-ring BPSK modulators, which modulate the MRM on either side of its resonance to induce a π phase shift [7–12]. These approaches are limited to two output levels per dimension and thus cannot be used for higher-order QAM modulation. Another set of approaches uses multiple MRMs and/or couplers to modulate amplitude and phase separately but these introduce high modulation loss making them unsuitable for high-bandwidth, low-BER links [13–16].

To address these shortcomings, we propose a novel offset-QAM-16 transmitter architecture using Ring-Assisted MZI (RAMZI) [17] structures. Previous works have introduced the RAMZI configuration to achieve low-chirp PAM modulators [18, 19], but do not demonstrate the RAMZI’s application for coherent communication (i.e. QAM-16). RAMZIs have been demonstrated for coherent communications in [20, 21], but these approaches rely on individual MRMs being biased at the laser wavelength, which has been shown to significantly reduce bandwidth [22, 23].

In this work, we use frequency-detuned RAMZIs to generate phase-constant amplitude modulators, which are the building

blocks of an offset-QAM transmitter capable of performing offset QAM-16 or higher-order coherent modulation. While offset has been typically suppressed for conventional QAM signaling, we show that the impacts of the offset will be minimal to OMA and bit errors induced by phase noise. In addition, we have recently exploited the offset signal to realize a DSP-free carrier recovery approach for QAM-16 [24]. Our work uses the O-band (1310 nm) because its low dispersion makes it the most practical choice for future intra-datacenter optical links [25].

This work includes a full circuit-level electro-optical modeling of the proposed transmitter, which we verify via simulation in an advanced silicon photonics process (Sections 2, 3). We then perform a link-level bit error rate (BER) modeling to demonstrate that RAMZI-based links can achieve target data rates with similar total optical powers as MZM-based links (Section 4). We also simulate and study the thermal stability of the MRMs for tuning and operation at the required optical power (Section 5).

We have validated this method using the GlobalFoundries (GF) 45 nm monolithic silicon photonics process (GF45SPCLO) [26] and show results in Section 6. In Section 7 we compare the RAMZI-based offset-QAM-16 (ROQ) transmitter (ROQ-T) with state-of-the-art solutions and show that it can achieve similar bit efficiencies to conventional MZM-based links while consuming $\sim 10\text{-}100\times$ lower area. We believe that this will enable the next generation of ultrafast, power- and area-efficient coherent CPO for realizing the vast potential of AI accelerators, GPUs, and network switches.

2. PROPOSED MRM-BASED COHERENT TRANSMITTER

The proposed RAMZI photonic circuit consists of two MRMs on either arm of an MZI (Fig. 2). Each MRM’s resonance wavelength can be thermally tuned to ensure that their resonances lie on opposite sides of the laser wavelength, and differential (i.e., push-pull) driving voltages are applied to simultaneously modulate the MRMs’ resonances in opposite directions towards or away from the laser wavelength (Fig. 3). This gives each MRM an identical amplitude change with opposite phase shift, which modulates the RAMZI’s output amplitude while holding output phase constant. A bias thermal phase shifter is included in one arm of the RAMZI. This can be tuned so that the individual MRM outputs interfere constructively in the high transmission state and destructively in the low transmission state. Thus, in addition to offering phase-constant operation, the RAMZI offers

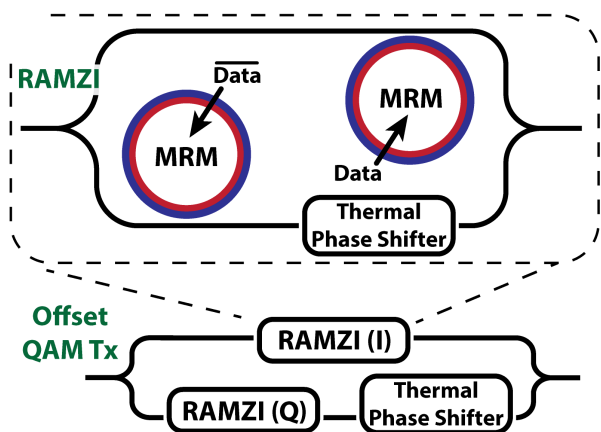


Fig. 2. Proposed RAMZI-based offset-QAM Transmitter and RAMZI photonic circuit.

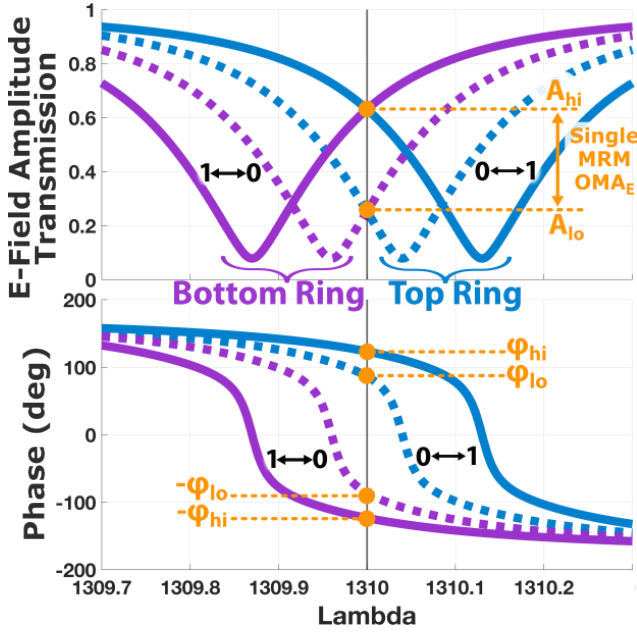


Fig. 3. Principle of operation for phase-constant RAMZI modulator.

an amplitude contrast superior to that of a single MRM by taking advantage of both amplitude and phase modulation in the MRM (Eq. 4). Two RAMZIs with separate data inputs can be combined with a $\pi/2$ phase shift to make an offset-QAM transmitter (Fig. 2).

Since the RAMZI has constant phase but variable power output, the constellation of a RAMZI-based transmitter is offset from the origin of the I-Q plane (Fig 4). Although unintuitive, the offset has been shown to be beneficial in realizing a DSP-free carrier phase recovery for QAM-16 [24], and has minimal impact to OMA and the impact of phase error on bit error rate (Sec. 3, 4). This offset is adjustable via tuning the bias points of each MRM to be closer to (less offset) or further from (more offset) the laser wavelength. When both MRMs are biased at the laser wavelength, QAM with no offset is performed. The offsets of I and Q branches can be tuned separately.

We let $A_T e^{i\phi_T}$ and $A_B e^{i\phi_B}$ be the output signal from the top and bottom MRMs, respectively, and let $\phi_{PS, Arm}$ be the phase shift of the thermal phase shifter after accounting for the $\pi/2$ phase delay of the bottom branch inherent to the output combiner. Since the MRMs always have opposite phases and equal amplitudes, we can represent ϕ_T and ϕ_B as ϕ_X and $-\phi_X$, and

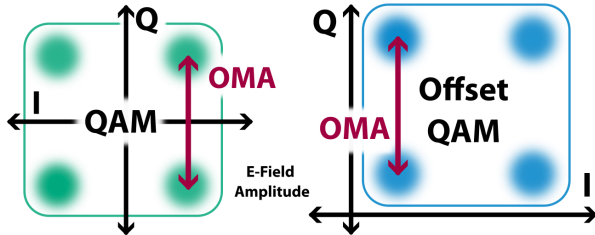


Fig. 4. Offset-QAM and QAM Constellations. In our proposed RAMZI-based transmitter, the offset is tunable and can be zero, to enable regular QAM operation

A_T and A_B as A_X . We calculate the output electrical field as:

$$E_{out} = \frac{1}{\sqrt{2}} (A_T e^{i\phi_T} + A_B e^{i(\phi_B - \phi_{PS})}) \quad (1)$$

We calculate RAMZI output phase ($\phi_{out,R}$) and power ($P_{out,R}$) as:

$$\begin{aligned} \phi_{out,R} &= \tan^{-1} \left(\frac{A_T \sin(\phi_T) + A_B \sin(\phi_B - \phi_{PS})}{A_T \cos(\phi_T) + A_B \cos(\phi_B - \phi_{PS})} \right) \\ &= \tan^{-1} \left(\frac{A_X}{A_X} \times \frac{\sin(\phi_X) + \sin(-\phi_X - \phi_{PS})}{\cos(\phi_X) + \cos(-\phi_X - \phi_{PS})} \right) \\ &= -\phi_{PS} \end{aligned} \quad (2)$$

$$\begin{aligned} P_{out,R} &\propto \frac{1}{2} (A_T^2 + A_B^2 + 2A_T A_B \cos(\phi_T - \phi_B + \phi_{PS})) \\ &\propto A_X^2 (1 + \cos(2\phi_X + \phi_{PS})) \end{aligned} \quad (3)$$

Equation 2 shows that output phase is constant. Since coherent optical receivers detect power proportional to the transmitted electric field strength, we calculate the effective optical modulation amplitude (OMA_E) of a device/circuit as the contrast between the output electric field amplitude in its high and low states. In this paper we will focus on the normalized OMA_E , in which all values are referenced to the RAMZI's electric field amplitude input. We let A_{Hi} , A_{Lo} , ϕ_{Hi} , ϕ_{Lo} be the MRM electric field amplitude (A_X) and phase output (ϕ_X) from Eqs. 2 and 3. We then calculate the RAMZI's OMA_E as:

$$\begin{aligned} OMA_E &= |E_{out,Hi}| - |E_{out,Lo}| \\ &= A_{Hi} \sqrt{1 + \cos(2\phi_{Hi} + \phi_{PS})} \\ &\quad - A_{Lo} \sqrt{1 + \cos(2\phi_{Lo} + \phi_{PS})} \end{aligned} \quad (4)$$

The OMA_E can be greatest when there is a large contrast between ϕ_{Hi} and ϕ_{Lo} . Maximum MRM output phase contrast might not occur at the same bias point as maximum MRM amplitude contrast. Thus, the bias point that maximizes the RAMZI's OMA_E may not be the one that maximizes the top and bottom MRMs' OMA_E .

The inherent wavelength selectivity of MRMs makes the RAMZI-based offset-QAM transmitter (ROQ-T) naturally adaptable for WDM operation. A WDM RAMZI can be constructed by placing multiple pairs of MRMs (each with their own resonance wavelength) on either arm of the same MZI so that a single thermal phase shifter in one arm is shared between them. This amortizes the area of the phase shifter over multiple wavelengths (4, 8, etc) to minimize overall transmitter area and make the area of a single RAMZI comparable to two single MRMs (i.e. those used in PAM operation).

While the coherent operation provided by ROQ provides a great benefit for intra-datacenter interconnect compared to MRM-based amplitude modulation, the underlying electro-optical devices (MRMs) the same. As a result, the existing peripheral electronics developed for MRM-based amplitude modulation can be used, facilitating ROQ adoption. This includes closed-loop thermal tuning of MRM resonance points with a drop port photodiode [27] as well as high-swing RF drivers for data modulation [28]. We address thermally tuning MRMs on both sides of resonance in Sec. 5.

3. SIMULATION METHODOLOGY AND RESULTS

We simulate the performance of the proposed photonic circuit using Spectre PDK models of the GF45SPCLO process in Cadence Virtuoso. These models include an MRM with a radius of

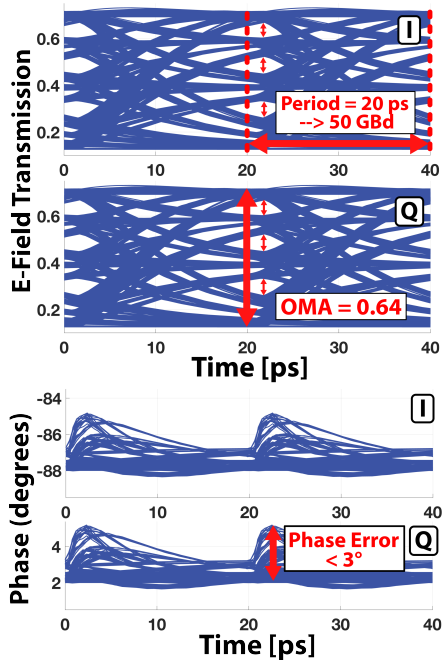


Fig. 5. Simulated electric field (E-field) amplitude (a) and phase (b) eye diagrams for the proposed RAMZI-based offset-QAM transmitter at 50 Gb/s.

$7.5 \mu\text{m}$ and $\sim 35 \text{ GHz}$ electro-optical bandwidth, as well as other photonic devices (e.g. thermal phase shifter, 1×2 MMI splitter, etc.). We use ideal 4-level PRBS voltage sources with 20% rise and fall times to drive all MRMs.

The first step is to find the correct thermal tuning levels for each MRM to maximize the RAMZI's OMA_E with each MRM resonance having an equal offset on opposite sides of the laser wavelength. We sweep the applied heat while applying a laser input in the O-band ($\sim 1310 \text{ nm}$) and 0V and -4V inputs to each MRM PN junction, which is the typical overall driving voltage swing for MRMs. By applying differential driving voltages to the MRMs, the RAMZI output amplitude is modulated while phase is held constant. For each combination of thermal tuning levels that give each MRM equal offsets on opposite sides of the laser wavelength, we sweep the RAMZI's arm phase shifter. Ultimately we pick the combination of MRM thermal tuning and RAMZI arm phase shift tuning that maximizes the RAMZI's OMA_E . Alternatively, this process could be done to optimize the RAMZI's offset level instead of the OMA_E , or a combination of the two.

We then find the pairs of intermediate driving voltages for top and bottom MRMs ($V_{\text{MRM},T}$, $V_{\text{MRM},B}$) that yield phase-constant RAMZI output electric field strengths evenly spaced between the high and low outputs found previously. Due to the nonlinearity of the MRM response with respect to applied voltage, as well as the dependence of RAMZI output on both amplitude and phase modulation in each MRM, this must be done iteratively. We sweep through all values of $V_{\text{MRM},T}$, $V_{\text{MRM},B}$ between 0 and -4 to find the combinations that yield equal amplitude shift and opposite phase shift in each MRM. For each, we calculate the RAMZI electrical field strength using the pre-determined arm phase shift. We then pick the combinations that yield RAMZI outputs with evenly-spaced electrical field strengths. This whole process up to this point is done at a very low laser power (-

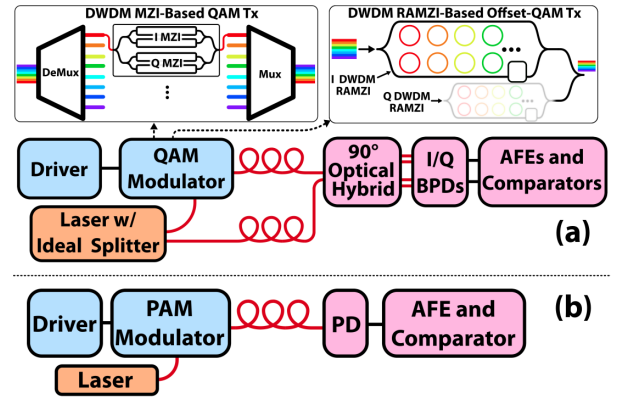


Fig. 6. Coherent laser-forwarded (a) and IM-DD (b) link architectures used for modeling link-level BER. The MZI-based transmitters require an additional wavelength mux and demux for WDM operation (mux/demux not shown in part b).

20 dBm input to each MRM) to make the effect of self-heating negligible.

The final step is to raise the laser power to the desired value for circuit operation. This may make self-heating no longer negligible, so we sweep the MRM thermal tuning power again to find the value that yields the optimal biasing points (temperatures) found earlier. We rapidly oscillate the the driving voltage at MHz speeds during the sweep to mimic realistic MRM tuning and operation. Although the driving voltage will oscillate at 10s of GHz speeds in realistic application, MHz speeds are sufficient because they are faster than the MRM thermal time constant ($\sim \text{ms}$).

We repeat the above process for a range of MRM input coupling gaps. For each, we measure the OMA_E in addition to the phase error, which is the maximum phase variations between any two of the four states. We pick a final coupling gap to maximize the RAMZI's OMA_E while maintaining a sufficiently low quality factor. Final Q values of ~ 3500 will support high-speed baud-rates of 50+ Gbd.

Our simulations show that after the arm phase shifter is properly tuned, the individual RAMZI can achieve an input-normalized OMA_E of 0.64 from four electric field transmission levels evenly spaced between 0.08 and 0.72 with a negligible phase error of $< 3^\circ$. The I/Q eye-diagrams of a RAMZI-based offset-QAM-16 transmitter are shown for amplitude (a) and phase (b) at an example baud-rate of 50 Gb/s for 200 Gb/s transmission in Fig. 5.

The multiple steps required for simulation methodology will not impede the efficiency and practicality of the proposed transmitter in actual datacenter applications. First, the driving voltages for multi-level operation ($V_{\text{MRM},T}$, $V_{\text{MRM},B}$) will be the same across MRMs in different transmitters and not change over time, so they only need to be calculated once. Second, while device temperature and thus the required heating power can fluctuate in actual applications due to external sources (i.e. thermal coupling with co-packaged GPU), power-efficient feedback-based thermal alignment and tuning of MRMs has been well studied and demonstrated in previous works [27].

4. LINK LEVEL MODELING

In order to demonstrate the effectiveness of the ROQ-T and compare to state-of-the-art solutions, we simulate the link-level bit

error rate (BER) as a function of total laser power for coherent and IM-DD formats with MZI- and MRM-based transmitters at target datarates of 200 and 400 Gb/s (per fiber per wavelength). For each we compare the performance of our ROQ-16 link to MZI-based PAM-4, PAM-8, QAM-4, and QAM-16 links, in addition to MRM-based PAM-4. System diagrams for QAM and PAM links are shown in Fig. 6.

For each combination of datarate and modulation format we calculate the appropriate baud rate, then calculate the peak-to-peak signal current at the receiver, and finally calculate the BER. The BER calculation takes into account peak-to-peak signal current, constellation geometry, receiver noise, and comparator threshold. The peak-to-peak signal current calculation takes into account coupler losses, link architecture, electro-optical modulator OMA/OMA_E and insertion loss, photodiode responsivity, optical mux/demux loss (only for MZI-based systems), and optical splitting/combination losses. We model the MRM with a 67 GHz bandwidth [29] and the MZM with a 100 GHz bandwidth, even though the best MZIs reported in literature have bandwidths between 60-80 GHz [30–33]. We assume all other circuit components to have infinite bandwidth. Full parameters used in modeling are shown in Tab. 1. We assume the MRM in the MRM-based PAM link to have an OMA of 0.4 and the RAMZI in the ROQ-16 link to have an OMA_E of 0.64, both based on simulation in the GF SPCLO process. We assume all MZIs to be fully driven (i.e. π phase shift in each arm for QAM, and $\pi/2$ in each arm for PAM).

To reflect the strict latency requirements of connected GPUs, we focus on optical power required to achieve a pre-FEC BER of 10^{-6} . This has been adopted for the next generation of PCIe communications and supports a low latency (\sim ns) [34]. The modeling results show that the ROQ-16 link can achieve the target pre-FEC BER at a total optical power of 6.71 and 9.65 dBm for 200 and 400 Gb/s links (Fig. 7a). For both datarates this optical power is within 1 dB of that required by QAM-16 MZI-based links and 5.3 and 7.7 dB less laser power than that required by a link based on the current CPO solution of MRM-based PAM-4. Although the modeling shows that for both datarates, MZI-based QAM-4 will achieve the lite-FEC BER with lower optical power, the high baud rate it requires will lead to immense electrical power and make it impractical for high datarate links.

To model the realistic operating environment of our proposed transmitter, we also simulate the effect of phase noise. Since in laser-forwarded CPO systems a single laser will be used to generate the LO and data signals used at the receiver, we anticipate that the path length mismatch between the two signals can be limited to 1 cm (due to fiber and on-chip waveguide mismatch). Based on commercially-available DFB O-Band lasers, we assume a laser linewidth of 1 MHz. These results are shown in Fig. 7b. Offset-QAM can be more susceptible to phase noise than non-offset-QAM because the offset-QAM constellation occupies a smaller range of the total I-Q phase space (Fig. 4). However, our simulation shows that even with phase noise taken into account, our ROQ-16 link can achieve the target pre-FEC BER at a total optical power within 2 dB of that required by QAM-16 MZI-based links. These results indicate the proposed link architecture using ROQ leads to 280 fJ/b laser energy-efficiency for both 200 Gb/s and 400 Gb/s (assuming 10% laser wall-plug efficiency [35, 36]).

Parameter	Value	Citation
Grating Coupler Insertion Loss	1.8 dB	[37]
Optical Mux (Demux) Loss	2.8 dB	[38]
Extra Link Margin	5 dB	
Photodiode Responsivity	1 A/w	[39]
MZI Insertion Loss	4 dB	[40]
RAMZI E-Field Offset [†]	0.42	Sim.
RAMZI OMA _E	0.64	Sim.
MRM OMA	0.4	Sim.
MZI OMA _E	2	[41]
MZI OMA	1	[41]
AFE Input-Ref Noise	15 pA/ $\sqrt{\text{Hz}}$	[42]
Input-Ref Comparator Threshold	(Bd Rate/50G) \times 5 μ A	[43]
MRM 3 dB Bandwidth	67 GHz	[29]
MZI 3 dB Bandwidth	100 GHz	[30]

Table 1. Parameters used in link-level BER modeling.

[†]The RAMZI E-field offset refers to the mean output E-field amplitude, relative to RAMZI input E-field amplitude.

5. THERMAL STABILITY DISCUSSIONS

RAMZI operation requires that the two MRMs be thermally biased with resonances on both the left and right side of the laser wavelength (Fig. 3). This deviates from how MRMs are traditionally used as transmitters, in which their resonance is placed on only the right side of the laser wavelength to ensure thermal stability by making the feedback between optical power and device temperature negative [44]. In order to ensure the thermal-stability of the RAMZI circuit for 200 and 400 Gb/s links, we simulate the thermal performance of the MRM at the requisite optical powers in our Spectre-based simulation Virtuoso environment.

To model a realistic MRM tuning application, we input various levels of optical power at a 1310 nm wavelength into a single MRM while rapidly applying 0V and -4V at 2 MHz. We sweep the thermal tuning voltage in both increasing and decreasing directions between 21 and 23.5 mW over 50 ms to modulate the resonance point of the MRM from below the laser wavelength to above it. These modulation speeds are chosen to model realistic MRM tuning by being higher (data modulation) or lower (thermal modulation) than the thermal time constant of the MRM (\sim 1 ms). In the resulting MRM E-field transmission we separate the points coming from the applied voltages of 0V and -4V. We then examine the outputs for thermal stability. The first sign of thermal stability is no bistability - that the MRM output must have a one-to-one relationship with heater power with no dependence on the direction from which that power is approached (i.e. heating vs cooling). The second sign of thermal stability is no metastability - during the thermal sweep the MRM output must change smoothly and continuously with no abrupt jumps.

Our simulation shows that the MRM features no thermal instability at input optical powers of less than or equal to -5 dBm (Fig. 8). The system-level optical powers of 6.7 and 9.7 dBm required for low-BER RAMZI-based offset-QAM-16 operation

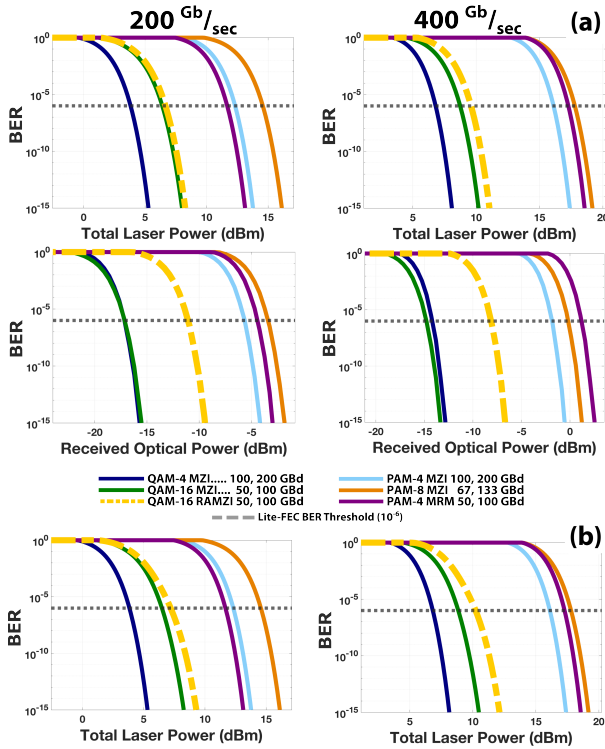


Fig. 7. Simulated BER as a function of laser optical power for a single channel in a single direction with a) no phase noise, b) laser linewidth of 1 MHz and a path length mismatch of 1 cm.

(Sec. 4, Fig. 7) equate to higher MRM input powers of -4.1 and -2.1 dBm. However, we believe that as power handling and dissipation of MRMs improve in coming years platforms (i.e. low loss waveguides in silicon), MRMs will be able to support these higher optical powers required for next-generation data rates of 200 and 400 Gb/s.

6. EXPERIMENTAL RESULTS

A proof of concept of the proposed offset-QAM optical transmitter is fabricated and validated using the GlobalFoundries 45 nm monolithic silicon photonics process (GF45SPCLO) [26]. For an electronic transmitter, the chip has custom-designed analog front ends (AFEs) consisting of CML-to-CMOS conversion and high-swing drivers using a VDD supply of 1.1V to support a 2V peak-to-peak drive voltage for MRMs. All MRMs are biased in full depletion mode. Thermal phase shifters and MRM heaters are controlled via external pulse density modulation (PDM) signals at a 48 MHz clock frequency from an FPGA. To demonstrate coherent amplitude modulation, the chip is designed to perform QAM-4 and not QAM-16.

The chip is wire-bond packaged directly on a PCB as shown in Fig. 9. The CML external data at 12.5 Gb/s was supported by a pattern generator and bit error rate test (BERT) equipment (Agilent J-BERT N4903A). Although all of the CMOS circuitry and MRMs can support up to 50 Gbd, reported data rates are currently limited by wire-bond packaging and equipment capabilities. In addition to on-chip Tx circuitry, we also implemented an on-chip coherent receiver (Rx) front-end using balanced photodetectors (BPD), a trans-impedance amplifier (TIA), and a CML buffer for quick debugging and calibration.

All optical circuits are designed to operate in the O-band

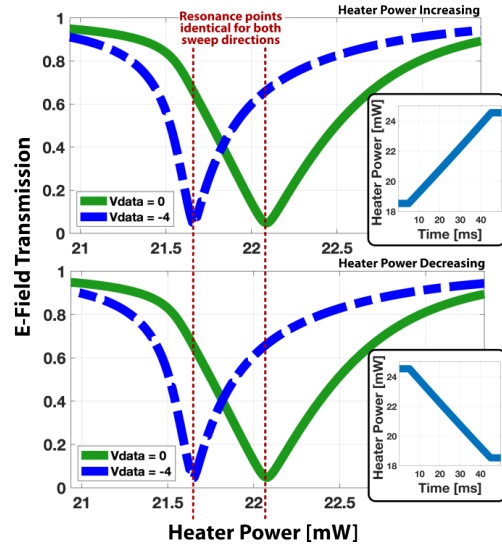


Fig. 8. The E-Field normalized transmission of an MRM as a function of heater power for both increasing and decreasing power directions.

(1310 nm), and MRMs have a radius of $7.5 \mu\text{m}$ with $\sim 45 \text{ pm/V}$ modulation efficiency and a Q-factor of 3500. Light is coupled into and out of the chip using grating coupler (GC) devices with $\sim 4 \text{ dB}$ loss in our current setup.

In order to tune all MRMs and phase shifters, we first swept the laser wavelength in the O-band and adjusted the MRMs thermally to separate their resonances by a fixed offset of $\sim 100 \text{ pm}$. We then applied the 12.5 GHz data and 2V MRM drivers and swept the laser to select the wavelength that yielded identical average power output in each MRM. We sensed MRM resonance points in this tuning process by connecting a high-precision voltage source to each MRM cathode to detect current proportional to optical power inside the MRM cavity. The final step was to sweep the power applied to the thermal phase shifter in each RAMZI and pick the value that maximized the observed OMA.

The I/Q eye diagrams at 12.5 Gb/s are shown in Fig. 10a. We characterize the BER as a function of total laser power for a single channel and show that our RAMZI-based offset-QAM transmitter can achieve the lite-FEC threshold of 10^{-6} with a RAMZI optical power input of -8 dBm (Fig 10b). These are all raw characterizations of the transmitter without using any equalization. The energy-efficiency is estimated to be 0.7 pJ/bit (including pre-drivers) for the overall 25 Gb/s offset-QAM-4 transmitter.

7. COMPARISON TO STATE-OF-THE-ART OPTICAL QAM-16 TRANSMITTERS

To demonstrate the energy and area efficiency of the ROQ-T relative to conventional approaches we compare our work to state-of-the-art MZI-based QAM transmitters made from Silicon, Indium Phosphide, and Thin-Film Lithium Niobate (TFLN) in Tab. 2. Since our fabricated chip was a proof of concept not optimized for CPO environments, we estimate the performance characteristics of our proposed transmitter based on reported results from literature on MRMs and MRM drivers for PAM-4 operation.

State-of-the-art 4-level (PAM-4) MRM drivers have been demonstrated with efficiency on the order of 50 fJ/bit [49]. Since

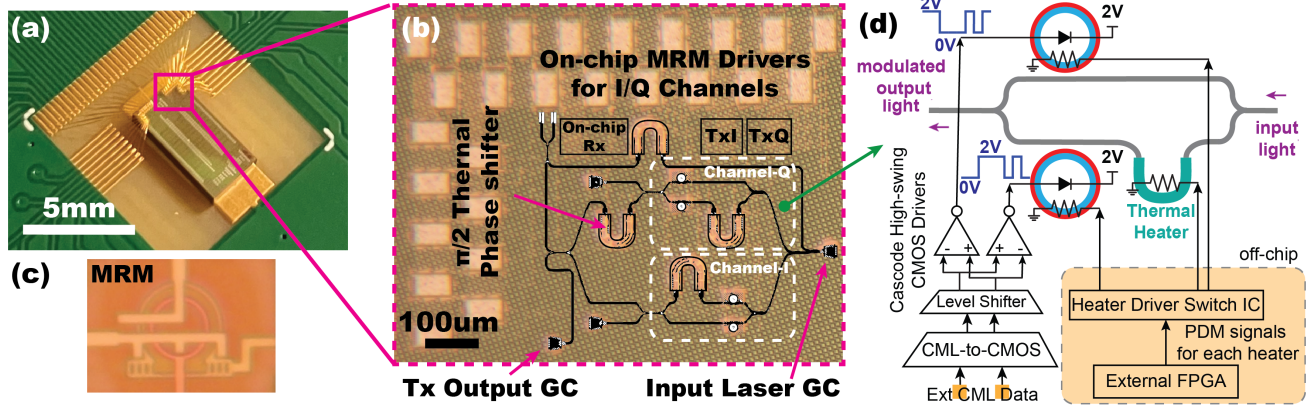


Fig. 9. (a) Photo of wire-bonded chip fabricated in GF45SPCLO, (b) optical transmitter area overlapped with photonic circuits, (c) micrograph of an MRM, and (d) block-diagram of on-chip driver and control CMOS circuitry.

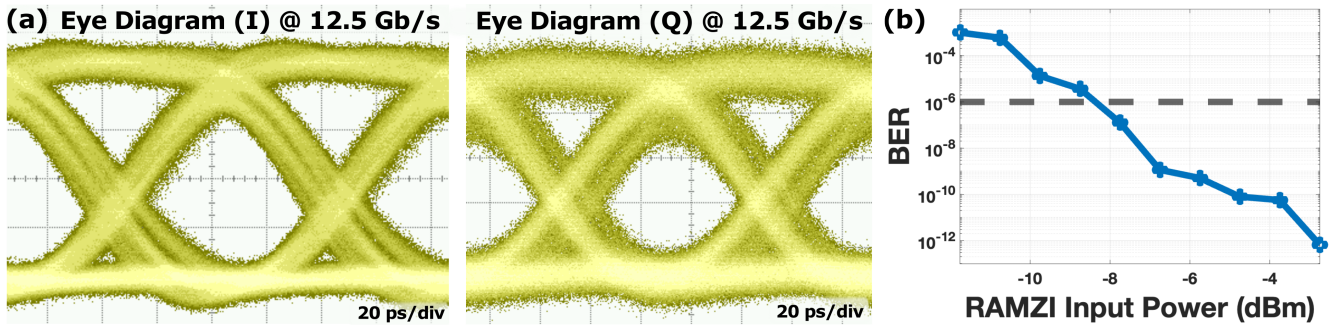


Fig. 10. (a) Measured I/Q eye-diagrams, and (b) characterized BER curves vs. RAMZI input optical power.

the ROQ-T will require two MRMs per dimension instead of one as is used for amplitude modulation, the efficiency will be roughly 100 fJ/bit. Meanwhile, MZM drivers for higher-order QAM operation have been demonstrated with efficiencies of 2-3 pJ/bit ([50, 51]).

Our work thus has a comparable power efficiency and data rate to MZM-based QAM-16 transmitters while providing more than 10-100 \times lower area. Compared to PAM-4 MRM-based transmitters, our work has similar area and electrical power efficiency but double the data rate per wavelength without increasing the baud rate or number of WDM laser lines. It also requires less laser power than PAM-4 MRM-based transmitters due to the higher sensitivity of coherent receivers (Fig. 7).

8. FUTURE WORK AND CONCLUSION

Co-packaged optics (CPO) is becoming imminent to meet the immense and growing demands of GPUs and network switches for rapid, dense, and energy-efficient optical intra-datacenter interconnect. However, shoreline density and thus overall data rates will be limited by the scaling of polarization and wavelength-division multiplexing as well as an ability of electronics to run at higher frequencies. Achieving target data rates for future datacenters of 400+ Gb/s per fiber per wavelength with high energy efficiencies can be achieved by using microring modulators for more advanced and coherent modulations.

In this work, we propose and demonstrate the usage of an O-band frequency-detuned ring-assisted Mach-Zehnder interferometer (RAMZI) for phase-constant amplitude transmission along with a RAMZI-based offset-QAM transmitter (ROQ-T).

We show its performance in a circuit-level simulation with devices from a leading silicon photonics process, achieving an input-normalized effective optical modulation amplitude of 0.64 per dimension while holding phase error below 3°. We conduct a full link-level modeling to show that it can achieve the target data rates with an optical power nearly identical to that required by conventional MZI-based modulators despite consuming \sim 10-100 \times less area. Additionally, we simulate its thermal properties to show its feasibility for operation at the required optical power. Finally, we demonstrate a proof of concept of our transmitter in the Global Foundries 45 nm silicon photonics process performing 25 Gb/s offset-QAM-4.

In the future we plan to demonstrate the presented approach across multiple channels at higher baud rates using on-chip clocking and pattern generation. Additionally, we will implement a closed-loop thermal sensing and control system to both align and lock MRM resonances to proper offsets on both sides of the laser wavelength, as is required for RAMZI operation. We have recently shown that offset-QAM modulation can be used to realize DSP-free, low-latency and energy-efficient C2PO link architectures [24], and will demonstrate this physically as well. With these future developments we will further demonstrate that RAMZIs and RAMZI-based offset-QAM transmitters will provide a compact and energy-efficient solution for CPO systems to continue scaling to meet the growing demands of GPUs, network switches, and datacenter interconnect at sustainable energy efficiencies.

Table 2. Comparison of state-of-the-art high-speed optical transmitters.

Platform, Work	Device	Modulation Format	Data Rate (Gb/s)	Baud Rate (GBd)	Area (mm ²)	Bandwidth (GHz)	$V_{\pi}L$ Efficiency (V · cm)
SOI [45]	MZI	QAM-16	400	120	3.5 [†]	37.7	NA
SOI [31]	MZI	QAM-64	556.8	116	4 [†]	63	3.6
TFLN [46]	MZI	QAM-32	533	128	23 [†]	60	2.9
InP [32]	MZI	QAM-16	400	128	NA	64	NA
InP [33]	MZI	QAM-16	576	144	12.5 [†]	90	2.5
SOI [47]	MRM	PAM-8	240	80	3.4e-3	110	0.825
SOI [48]	MRM	PAM-4	240	120	6.4e-5	54	0.53
This Work [‡]	MRM	QAM-16	400	100	2e-2	110	0.825
This Work [¶]	MRM	QAM-4	25	12.5	0.2	NA	0.5

[†] Area is estimated from reported device length by assuming an MZI width of 0.5 mm.

[‡] Theoretical analysis: bandwidth and efficiency obtained from reported literature on MRM-based transmitters. Area estimate based on a 4λ WDM RAMZI-based QAM Tx developed in the GF 45 nm SPCLO process in which one thermal phase shifter is shared for all MRMs in each I/Q modulator.

[¶] Experimental results.

REFERENCES

- R. Mahajan, X. Li, J. Fryman, *et al.*, "Co-packaged photonics for high performance computing: Status, challenges and opportunities," *J. Light. Technol.* **40**, 379–392 (2022).
- J. He, Y. Zhang, H. Liu, *et al.*, "A 56-gb/s reconfigurable silicon-photonics transmitter using high-swing distributed driver and 2-tap in-segment feed-forward equalizer in 65-nm cmos," *IEEE Trans. on Circuits Syst. I: Regul. Pap.* **69**, 1159–1170 (2022).
- "Universal chiplet interconnect express (ucie) specification," Tech. rep. (2024).
- P. J. Winzer, "The future of communications is massively parallel," *J. Opt. Commun. Netw.* **15**, 783–787 (2023).
- D. D. Sharma, G. Pasdast, S. Tiagaraj, and K. Aygün, "High-performance, power-efficient three-dimensional system-in-package designs with universal chiplet interconnect express," *Nat. Electron.* **7**, 244–254 (2024).
- L. A. Valenzuela, Y. Xia, A. Maharry, *et al.*, "A 50-gbaud qpsk optical receiver with a phase/frequency detector for energy-efficient intra-data center interconnects," *IEEE Open J. Solid-State Circuits Soc.* **2**, 50–60 (2022).
- N. Mehta, S. Lin, B. Yin, *et al.*, "A laser-forwarded coherent 10gb/s bpsk transceiver using monolithic microring resonators in 45nm soi cmos," in *2019 Symposium on VLSI Circuits*, (2019), pp. C192–C193.
- Y. Jo, M. Oberon, A. Peczek, *et al.*, "Novel monolithic all-silicon coherent transceiver sub-assembly based on ring modulators," *J. Light. Technol.* pp. 1–10 (2024).
- S. Debnath, S. Das, N. Sinha, *et al.*, "Generation of an optical 8-amplitude phase shift keying modulator using silicon microrings in add-drop configuration," *Opt. Eng.* **63**, 035110 (2024).
- P. Dong, C. Xie, L. L. Buhl, and Y.-K. Chen, "Silicon microring modulators for advanced modulation formats," in *2013 Optical Fiber Communication Conference and Exposition and the National Fiber Optic Engineers Conference (OFC/NFOEC)*, (2013), pp. 1–3.
- K. Padmaraju, N. Ophir, Q. Xu, *et al.*, "Error-free transmission of dpsk at 5 gb/s using a silicon microring modulator," in *2011 37th European Conference and Exhibition on Optical Communication*, (2011), pp. 1–3.
- K. Padmaraju, N. Ophir, S. Manipatruni, *et al.*, "Dpsk modulation using a microring modulator," in *CLEO:2011 - Laser Applications to Photonic Applications*, (2011), p. CTuN4.
- Y. Ehrlichman, O. Amrani, and S. Ruschin, "Generating arbitrary optical signal constellations using microring resonators," *Opt. Express* **21**, 3793 (2013).
- W. D. Sacher and J. K. S. Poon, "Microring quadrature modulators," *Opt. Lett.* **34**, 3878 (2009).
- S. Karimelahi and A. Sheikholeslami, "Quadrature amplitude modulation (qam) using binary-driven coupling-modulated rings," *Opt. Commun.* **366**, 354–361 (2016).
- W. D. Sacher, W. M. J. Green, D. M. Gill, *et al.*, "Binary phase-shift keying by coupling modulation of microrings," *Opt. Express* **22**, 20252–20259 (2014).
- J. Cardenas, P. A. Morton, J. B. Khurgin, *et al.*, "Linearized silicon modulator based on a ring assisted mach zehnder interferometer," *Opt. Express* **21**, 22549 (2013).
- R. Li, D. Patel, E. El-Fiky, *et al.*, "High-speed low-chirp pam-4 transmission based on push-pull silicon photonic microring modulators," *Opt. Express* **25**, 13222 (2017).
- X. Wu, D. Huang, R. Kumar, *et al.*, "Fully integrated silicon photonic high-speed transmitter with ring-assisted mach-zehnder modulator," in *2024 Optical Fiber Communications Conference and Exhibition (OFC)*, (2024), pp. 1–3.
- A. Geravand, Z. Zheng, F. Shateri, *et al.*, "Ultrafast coherent dynamics of microring modulators," (2024).
- A. Geravand, Z. Zheng, S. Lévassieur, *et al.*, "Ultra-compact silicon iq modulator beyond 100 gbaud," in *49th European Conference on Optical Communications (ECOC 2023)*, vol. 2023 (2023), pp. 1524–1526.
- H. Yu, D. Ying, M. Pantouvaki, *et al.*, "Trade-off between optical modulation amplitude and modulation bandwidth of silicon micro-ring modulators," *Opt. Express* **22**, 15178 (2014).
- H.-C. Kao, M.-W. Lin, and M.-C. M. Lee, "Study of electrical and optical peaking of si ring modulators for tailoring modulation band," *IEEE Photonics J.* **15**, 1–6 (2023).
- M. Rezaei, D. Sturm, P. Zeng, and S. Moazeni, "Dsp-free carrier phase recovery system for laser-forwarded offset-qam coherent optical receivers," in *2024 IEEE 67th International Midwest Symposium on Circuits and Systems (MWSCAS)*, (2024), pp. 1158–1161.
- M. Kanellos, "O-band optics: A new market for optimizing the cloud," (2024).
- M. Rakowski, C. Meagher, and K. N. *et al.*, "45nm cmos - silicon photonics monolithic technology (45clo) for next-generation, low power

- and high speed optical interconnects," in *Optical Fiber Communication Conference (OFC) 2020*, (2020), p. T3H.3.
27. H. Li, G. Balamurugan, T. Kim, *et al.*, "A 3-d-integrated silicon photonic microring-based 112-gb/s pam-4 transmitter with nonlinear equalization and thermal control," *IEEE J. Solid-State Circuits* **56**, 19–29 (2021).
 28. J. Sharma, Z. Xuan, H. Li, *et al.*, "Silicon photonic microring-based 4 × 112 gb/s wdm transmitter with photocurrent-based thermal control in 28-nm cmos," *IEEE J. Solid-State Circuits* **57**, 1187–1198 (2022).
 29. Y. Zhang, H. Zhang, M. Li, *et al.*, "200 gbit/s optical pam4 modulation based on silicon microring modulator," in *2020 European Conference on Optical Communications (ECOC)*, (2020), pp. 1–4.
 30. Y. Ogiso, J. Ozaki, Y. Ueda, *et al.*, "Ultra-high bandwidth inp iq modulator for beyond 100-gbd transmission," in *2019 Optical Fiber Communications Conference and Exhibition (OFC)*, (2019), pp. 1–3.
 31. Z. Zheng, A. Mohammadi, X. Zhang, *et al.*, "Net 556.8 gbps/pol coherent transmission enabled by a two-segment all-silicon modulator," in *2022 European Conference on Optical Communication (ECOC)*, (2022), pp. 1–4.
 32. Y.-W. Chen, K. Kuzmin, R. Zhang, *et al.*, "Inp cdm and icr enabled 128gbaud/ dp-16qam-ps and 120gbaud/dp-qpsk long-haul transmission," *IEEE Photonics Technol. Lett.* **34**, 471–474 (2022).
 33. J. Ozaki, Y. Ogiso, Y. Hashizume, *et al.*, "Over-85-ghz-bandwidth inp-based coherent driver modulator capable of 1-tb/s/ λ -class operation," *J. Light. Technol.* **41**, 3290–3296 (2023).
 34. D. D. Sharma, "The pcie 6.0 specification webinar q&a: Error detection and correction with fec," (2024).
 35. H. Shu, L. Chang, Y. Tao, *et al.*, "Microcomb-driven silicon photonic systems," *Nature* **605**, 457–463 (2022).
 36. D. Huang, Z. Xuan, R. Kumar, *et al.*, "A silicon photonic 8λ , x 32gbps/ λ , wdm transceiver with integrated laser array and soa for optical i/o," *2023 Int. Electron Devices Meet. (IEDM)* pp. 1–4 (2023).
 37. Y. Luo, Z. Nong, S. Gao, *et al.*, "Low-loss two-dimensional silicon photonic grating coupler with a backside metal mirror," *Opt. Lett.* **43**, 474–477 (2018).
 38. J. A. Davis, A. Li, N. Alshamrani, and Y. Fainman, "Silicon photonic chip for 16-channel wavelength division (de-)multiplexing in the o-band," *Opt. Express* **28**, 23620 (2020).
 39. F. Bozorgi, M. Bruccoleri, E. Rahimi, *et al.*, "Analog front end of 50-gb/s sige bicmos opto-electrical receiver in 3-d-integrated silicon photonics technology," *IEEE J. Solid-State Circuits* **57**, 312–322 (2022).
 40. E. El-Fiky, A. Samani, D. Patel, *et al.*, "400 gb/s o-band silicon photonic transmitter for intra-datacenter optical interconnects," *Opt. Express* **27**, 10258 (2019).
 41. X. Zhou, R. Urata, and H. Liu, "Beyond 1 tb/s intra-data center interconnect technology: Im-dd or coherent?" *J. Light. Technol.* **38**, 475–484 (2020).
 42. G. Kalogerakis, T. Moran, T. Nguyen, and G. Denoyer, "A quad 25gb/s 270mw tia in 0.13 μm bicmos with <0.15 db crosstalk penalty," in *2013 IEEE International Solid-State Circuits Conference Digest of Technical Papers*, (2013), pp. 116–117.
 43. K. T. Settaluri, C. Lalau-Keraly, E. Yablonovitch, and V. Stojanović, "First principles optimization of opto-electronic communication links," *IEEE Trans. on Circuits Syst. I: Regul. Pap.* **64**, 1270–1283 (2017).
 44. M. de Cea, A. H. Atabaki, and R. J. Ram, "Power handling of silicon microring modulators," *Opt. Express* **27**, 24274–24285 (2019).
 45. J. Wang, M. Al-Qadi, W.-J. Jiang, *et al.*, "120-gbaud 16-qam silicon photonics iq modulator for data center interconnection," *Opt. Express* **31**, 25515 (2023).
 46. E. Berikaa, M. S. Alam, and D. V. Plant, "Unamplified coherent transmission of net 500 gbps/polarization/ λ for intra-datacenter interconnects," *IEEE Photonics Technol. Lett.* **34**, 1135–1138 (2022).
 47. Y. Zhang, H. Zhang, J. Zhang, *et al.*, "240 gb/s optical transmission based on an ultrafast silicon microring modulator," *Photon. Res.* **10**, 1127–1133 (2022).
 48. M. Sakib, R. Kumar, C. Ma, *et al.*, "A 240 gb/s pam4 silicon micro-ring optical modulator," in *2022 Optical Fiber Communications Conference and Exhibition (OFC)*, (2022), pp. 01–03.
 49. S. Moazeni, S. Lin, M. Wade, *et al.*, "A 40-gb/s pam-4 transmitter based on a ring-resonator optical dac in 45-nm soi cmos," *IEEE J. Solid-State Circuits* **52**, 3503–3516 (2017).
 50. Y.-L. Luo, R. Rady, K. Entesari, and S. Palermo, "A power-efficient 20–35-ghz mzm driver with programmable linearizer for analog photonic links in 28-nm cmos," *IEEE Trans. on Microw. Theory Tech.* **71**, 1262–1273 (2023).
 51. Y. Sobu, G. Huang, T. Mori, *et al.*, "Highly power-efficient (2 pj/bit), 128gbps 16qam signal generation of coherent optical dac transmitter using 28-nm cmos driver and all-silicon segmented modulator," in *2022 Optical Fiber Communications Conference and Exhibition (OFC)*, (2022), pp. 1–3.